X-ray diffraction (H-RHA-SBA-16, Al-RHA-SBA-16, TI-RHA-SBA-16)

This section gives detailed information on characterization data of the H-RHA-SBA-16, Al-RHA-SBA-16 and Ti-RHA-SBA-16 samples with different Si/Al ratios and with different wt.% of Ti- exchanged respectively.The XRD patterns of the calcined parent H-RHA-SBA-16 Al-RHA-SBA-16 and Ti-RHA-SBA-16 samples with different Si/Al ratios (4, 7 and 9) and with different wt.% of Ti (2wt.%, 4wt.% and 6wt.%) respectively are presented in Fig. 2 (A, B, C) respectively. The spectra showed XRD patterns identical to that reported for standard SBA-16 materials. Beck*et al.* indexed these peaks for a hexagonal unit cell, the parameter of which was calculated from the equation $a_0 = \sqrt{2}d_{110}$.

On calcination of samples, the peak is shifted to lower d_{110} spacing value probably due to condensation of internal Si-OH groups giving rise to a contraction of the unit cell. The unit cell parameter and d-spacing of the Al-RHA-SBA-16, Ti-RHA-SBA-16 samples and H-RHA-SBA-16 are given in Table 2. The slight increase in d-spacing and unit cell parameters of both Al-RHA-SBA-16 and Ti-RHA-SBA-16 compared to H-RHA-SBA-16 suggests the presence of Aluminum and Titanium in the framework respectively. The increase in unit cell parameter on Al or Ti incorporation is probably due to the replacement of shorter Si-O bonds by longer Al-O and Ti-O bonds in the structure respectively. It is also observed that along with an increase in the unit cell parameter, the (110) diffraction peak becomes broader and less intense with increasing Aluminum or Titanium content, probably because of the change of the Al-O-Al and Ti-O-Ti bond angle, causing a distortion in the long range ordering of the hexagonal mesoporous structure.

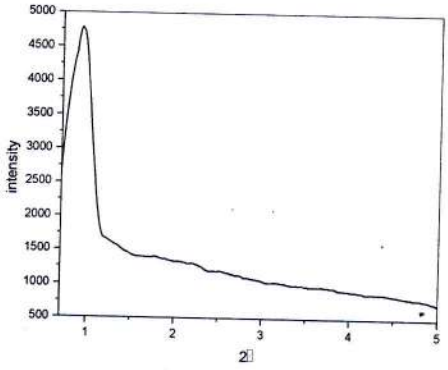

(A)

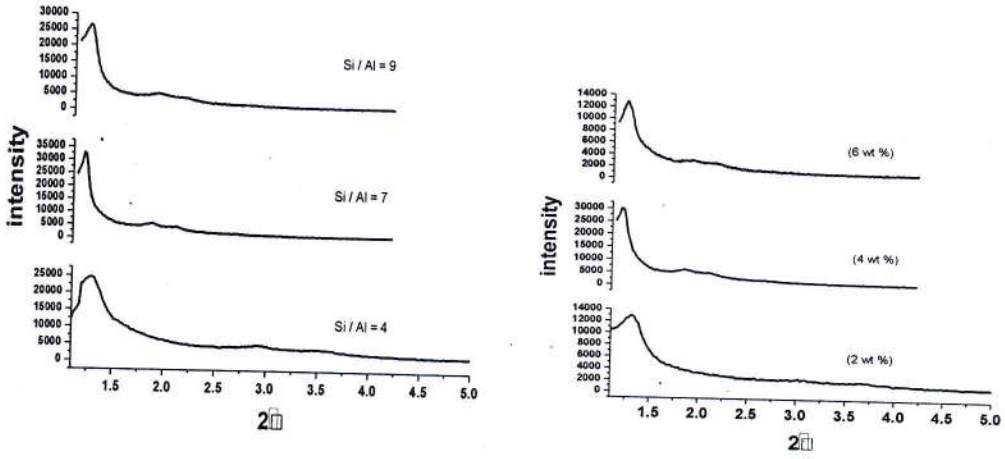

(B) (C)

Fig. 2 A) XRD patterns of calcined parent H-RHA-SBA-16sample. B)Al-RHA-SBA-16 (i.e. Si/Al=4, 7, 9)
C) Ti-RHA-SBA-16 (i.e.2wt.%, 4wt.% and 6wt.%)

Co-ordinator IQAC

PRINCIPAL

Fig. 2. (B, C) illustrate that in all the modified forms of H-RHA-SBA-16 sample, there are marginal changes in the crystallinity but almost no changes in the phase purity and structural morphology are being observed after modification with different amounts of $Al^{+++}$and Ti^{++} percentage. This indicates the structural stability of the parent sample and presence of metal ions in the intra-crystalline voids of the H-RHA-SBA-16. The percent crystallinity of the samples is drawn with the amount of metal ion percent in them. From the Table 2.as the metal ions percent increases in modification, an increase in the crystallinity of the samples was observed up to Si/Al=4 and 6wt% of Ti. But when Si/Al > 4 and Ti incorporation is more than 6wt% i.e. when the metal ion concentration increases then the sample declines from good crystallinity to amorphous nature. This is because of the fact that, Al itself is having an amorphous nature and Ti being strong earth metal it produces other amalgamations in the structure influencing the crystallinity, hence the modification was stopped after Si/Al=4 and more than 6wt% of Ti incorporation to retain the crystallinity of the sample. The crystallinity of the sample was 100% for H-RHA-SBA-16.If the 'Al' metal ion concentration in H-RHA-SBA-16 was Si/Al = 4 crystallinity was 98.5% and then gradually decreased for Si/Al=7, 9 as 91.3% and 86.5% respectively. However, if the 'Ti' metal ion concentration in H-RHA-SBA-16 was 6wt%, it was 96.5% and then gradually decreased for 4wt% and 2wt% as 84.3% and 80.4% respectively.

Fig. 3.depicts the co-relation between % crystallinity and concentration of Al and Ti metal ions.

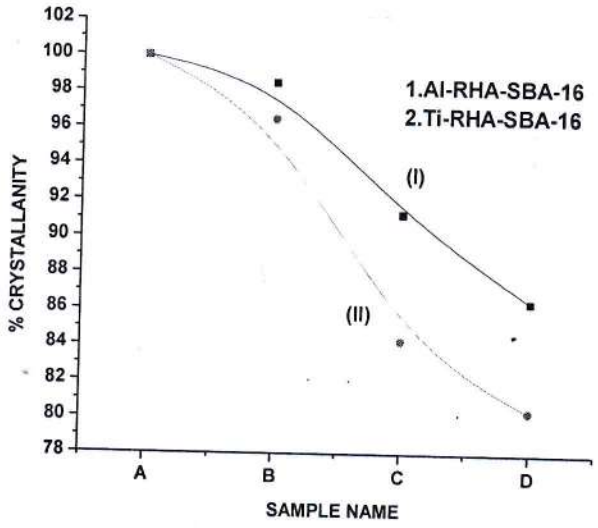

Fig.3 Effect of the metal concentration on Percent CrystallinityofH-RHA-SBA-16

Furthermore, XRD patterns recorded at higher angles up to 80^0 showed no peaks. Therefore, the presence of any crystalline Al or Ti containing species can be excluded.

Table 2 Physicochemical properties of Al-RHA-SBA-16 and Ti-RHA-SBA-16 samples

Sample	d_{110}	Surface Area(m^2/g)	Pore Volume (ml/g)	Pore diameter(A^0)	% Crystallanity	Acidity (mmole/g)
H-RHA-SBA-16	33.16	954.22	0.65	27.3	100	0.014
Al-RHA-SBA-16 (Si/Al=4)	33.32	852.00	0.76	28.6	98.5	0.192
Al-RHA-SBA-16 (Si/Al=7)	34.62	826.46	0.71	31.2	91.3	0.086
Al-RHA-SBA-16 (Si/Al=9)	35.75	938.61	0.69	26.8	86.5	0.044

Ti-RHA-SBA-16 (2wt%)	45.56	789.36	0.62	30.9	80.4	0.017
Ti-RHA-SBA-16 (4wt%)	45.85	809.58	0.68	30.4	84.3	0.019
Ti-RHA-SBA-16 (6wt%)	45.58	926.25	0.72	29.8	96.5	0.024

Sorption studies:

The BET surface areas, average pore diameters and pore volumes calculated from N_2-sorption isotherms of Al-RHA-SBA-16 (Si /Al = 4, 7, 9) and Ti-RHA-SBA-16 (2wt%, 4wt%, 6wt%) presented in Table 2. According to IUPAC classification, the isotherms are of type IV[68] presented for Al-RHA-SBA-16 (Si /Al = 4, 7, 9) and Ti-RHA-SBA-16 (2wt%, 4wt%, 6wt%) in Fig. 4. (A, B) and 5.(A, B) respectively.

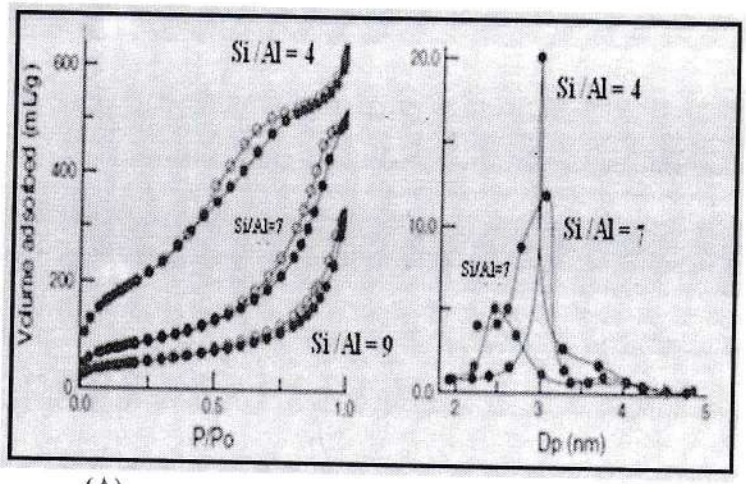

(A) (B)

Fig. 4.A) N_2-adsorption-desorption isotherms and (B) Pore size distribution of Al-RHA-SBA-16(Si /Al = 4, 7, 9)

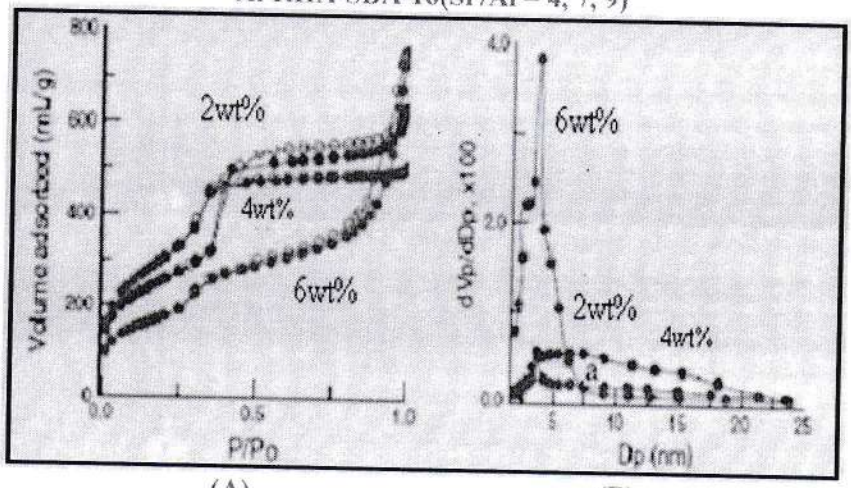

(A) (B)

Fig. 5.A) N_2-adsorption-desorption isotherms and (B) Pore size distribution of Ti-RHA-SBA-16(2wt%, 4wt%, 6wt%)

The position of p/p_0 at which inflection starts is related to the diameter of the mesopores. The sharpness in this step indicates the uniformity of the pore size distribution. In the case of both M-RHA-SBA-16 (M = Al or Ti), this step of isotherm shifts slightly towards higher relative pressure p/p_0 with increase in

Co-ordinator PRINCIPAL

metal content of the sample indicating increase in the pore size. However, broadening of the hysteresis loop increases with increase in the metal content. This may be due to changes in the contour of the mesopores.The hysteresis loop in the range of $p/p_0 > 0.8$ due to capillary condensation in the inter-particle mesopores is observed in case of M-RHA-SBA-16. A comparison of the hysteresis loops of these two sets of samples at higher relative pressure region indicates difference in their textural mesoporosity. The pore diameters increase with increasing metal (Al or Ti) content of the samples.

Temperature Programmed Desorption of Ammonia

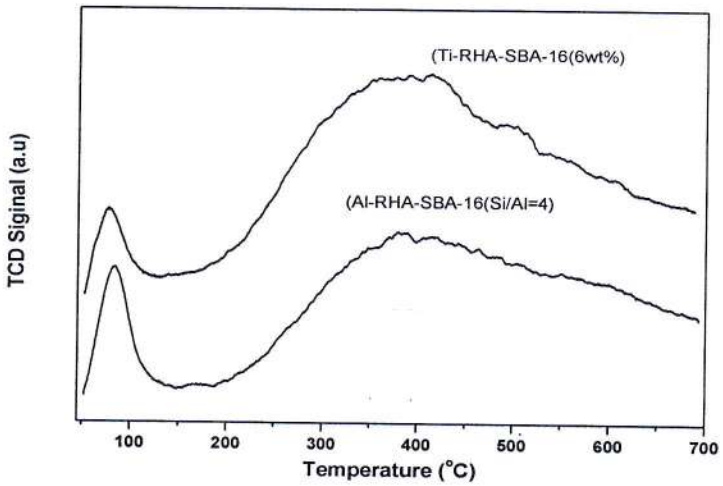

Fig.6. Temperature Programmed Desorption of Ammonia of Ti-RHA-SBA-16

The acidities of the H-Al-SBA-16 samples were characterized by the TPD of Ammonia. The acid strengths appear to be rather moderate as nearly all the Ammonia desorbed below 250^{0}C.The acidities (mmol/g) based on the Ammonia desorbed by the samples beyond 90^{0}C are presented in Table 2.

As the Aluminum content increases, the total acidity increases in the samples (Al-RHA-SBA-16(Si/Al=9) <Al-RHA-SBA-16(Si/Al=7) <Al-RHA-SBA-16 (Si/Al=4). However as the Titanium content increases, the total acidity decreases in the samples (Ti-RHA-SBA-16 (2wt%)< Ti-RHA-SBA-16 (4wt%) < Ti-RHA-SBA-16 (6wt %)).

SEM

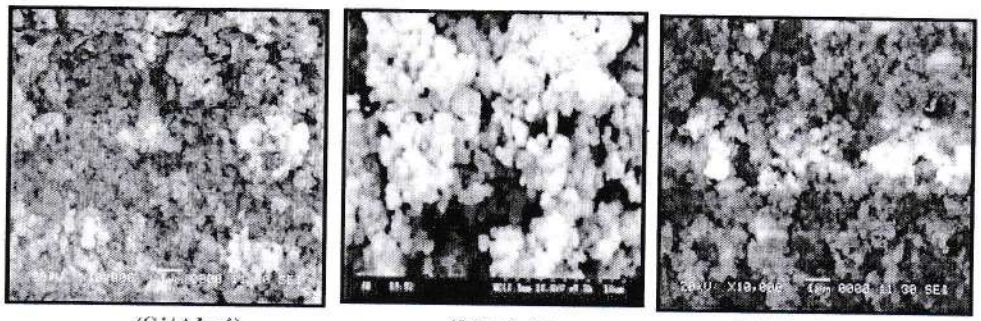

(Si/Al=4) (Si/Al=7) (Si/Al=9)

Fig. 7.Scanning electron micrograph of Al-RHA-SBA-16.

Co-ordinator IQAC

Shri Guru Buddhiswami Shikshan Prasarak Sanstha's Shri Guru Buddhiswami Mahavidyalaya Purna

PRINCIPAL

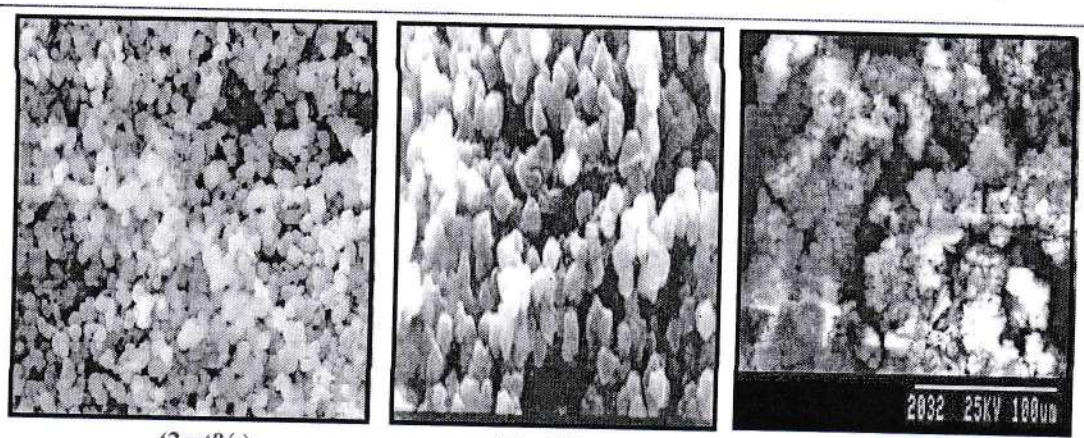

(2wt%) (4wt%) (6wt%)

Fig. 8. Scanning electron micrograph of Ti-RHA-SBA-16.

Scanning electron micrographs of all the modified Al-RHA-SBA-16 (Si/Al=4, 7, 9) and Ti-RHA-SBA-16 (2, 4, 6wt %) samples is presented in Fig. 7.and Fig. 8.respectively. The micrographs reveal two morphologies, such as hexagonal and spherical habit and majority of them are hexagonal shaped agglomerates of small particles of the size between 3.10–10.60A^0.It is seen that the morphology of the crystals gets affected as the metal ion percent gradually increased. The SEM photograph of H-RHA-SBA-16 sample shows bigger crystal size while the modified forms the metal ions have decreased crystal size which may affect the surface properties of the H-RHA-SBA-16 which tend to use it for different applications.

FTIR

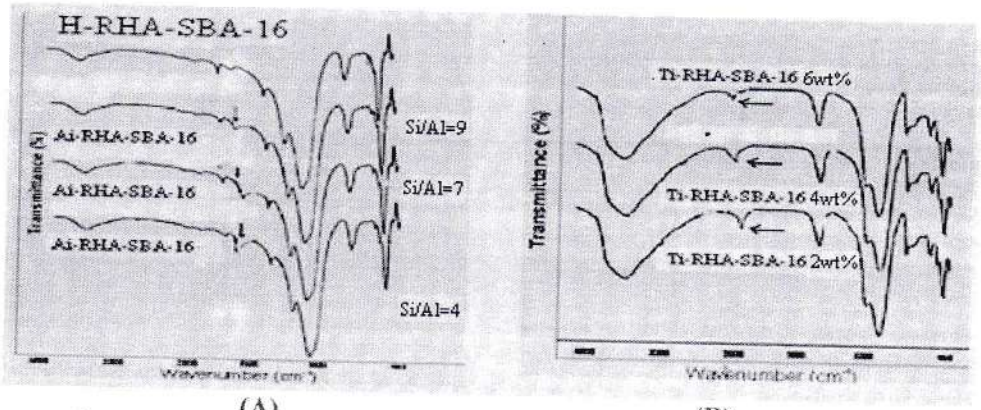

(A) (B)

Fig.9.FTIR spectra of calcinedH-RHA-SBA-16 and its modified forms with Al^{+++} and Ti^{++} ions.

The IR spectra of lattice vibration of calcined H-RHA-SBA-16 Al-RHA-SBA-16 and Ti-RHA-SBA-16 are presented in (Fig. 9.(A, B)). The spectra shows four main absorption bands between the regions 1210-1230, 1045-1080, 790-815 and 440-470 cm^{-1}. The T-O-T lattice vibrations are found to shift to lower wave numbers for Al-RHA-SBA-16 probably due to the incorporation of Al into the channel walls, as Al-O bond is longer than Si-O bond.

The band in the region 1210 to 1230 cm^{-1} is due to external asymmetric stretching vibrations of five member Si-O rings, which is an evidence for the presence of 8 member rings in the walls of SBA-16 structure. This band becomes less intense in the calcined samples indicating probably a rearrangement of the wall structure due to high temperature treatment.

The band in the region 1045-1090 cm^{-1}due to internal asymmetric stretching mode of $SiO_4(TO_4)$ skeleton appears to be the strongest band in the spectra of all silicates. The broadening of this band on calcination may be due to superimposition of many bands ascribable to TO_4 arising from different T-O-T angles, this band is significantly shifted to a lower wave number (1066cm^{-1}). This may be due to the stretching

Co-ordinator

PRINCIPAL

of Si-O bond by long chain surfactant molecules forming micelles around which the SiO4 species are wound during formation of the mesoporous molecular sieves. Interestingly, this band at~ 1066 cm^{-1} of mesoporous molecular sieves is found to be shifted to the higher wave number i.e.~1085 cm^{-1} on removal of the surfactant molecules during calcination. This suggests that contraction of Si-O bond takes place during calcination, which has also been confirmed by XRD characterization.All IR spectra exhibit one common feature, a band at ~970 cm^{-1}. The correct interpretation of this vibrational band has been a matter of extensive studies. Fig.9. shows that within corporation of metal ions, the intensity of this band marginally increases. This band is generally considered as a proof for the incorporation of the heteroatom into the framework.

REFERENCES:

1. G. Ferraiolo, M. Zilli, A. Converti, Fly ash disposal and utilization, *J. Chem. Technol. Biotechnol.*47, 281–305, **(1990).**
2. C.L. Carlson, D.C. Adriano, Environmental impact of coal combustion residue, *J. Environ. Qual.* 22, 227–247, **(1993).**
3.. KekaOza, Narayan C Pradhan; AmarnathSamanta*Bull Matter science.*,Vol.27 pp 555-564, **(2004).**
4.. Coal Resources of India S. Farooq Department of Geology AMU.
5.. Adler KB, Mossman BT, Butler GB, Jean LM, Craighead JE Interaction of Mount St. Helens' volcanic ash with cells of the respiratory epithelium. *Environ Res* 35:346–361, **(1984).**
6. Akematsu T, Dodson RF, Williams MG, Hurst GA, The short-term effects of volcanic ash on the small airways of the respiratory system. *Environ Res* 29:358–370, **(1982).**
7. Baxter PJ The eruption of El Reventador volcano 2002: health hazards and the implications for volcano risk management in Ecuador. Report to the *Pan-American Health Organization, Pan American Health Organization, Washington DC***(2003).**
8. Baxter PJ, Ing R, Falk F, French J, Stein GF, Bernstein RS, Merchant JA, Allard J Mount St Helens eruptions, May 18 to June 12 1980. *J Am Med Assoc* 246: 2585–2589, **(1981).**
9. Baxter PJ, Woo G, Pomonis A Preliminary assessment of volcanic risk on Montserrat.*Montserrat Volcano Observatory, Montserrat*, p 32, **(1998).**
10. Baxter PJ, Bonadonna C, Dupree R, Hards VL, Kohn SC, Murphy MD, Nichols A, Nicholson RA, Norton G, Searl A, Sparks RSJ, Vickers BP Cristobalite in volcanic ash of the *Soufrière Hills Volcano, Montserrat, British West Indies. Science* 283:1142–1145, **(1999).**
11. FAO Food Outlook, *Food and Agriculture Organization of the United Nations*, November, **(2011).**
12. ERIKSON, S. and PRIOR, M., *"The Briquetting of Agricultural Waste for Fuel"*, FAO Environment and Energy paper 11, FAO of the UN, Rome. **(1990).**
13. Corma, *A. Chem. Rev.* 95, 559-614, **(1995).**
14. Mirodatos, C.; Barthomeuf, D. *J. Catal.*93, 246, **(1985).**
15. Wilson, S. T.; Lok, B. M.; Flanigen, E. M. *U.S. Patent* 4,310,440, **(1982).**
16. Dessau, R. M.; Schlenker, J. L.; Aiggins, *J. B. Zeolites*, 10, 522, **(1990).**
17. Kresge, C. T.; Leonowicz, M. E.; Roth, W. J.; Vartulli, J. C.; Beck, J. S. *Nature* 359, 710, **(1992).**
18. Beck, J. S.; Chu, C. T.; Johnson, I. D.; Kresge, C. T.; Leonowicz, M. E.; Roth, W. J.; Vartulli, J. C. U.S. Patent 5,108,725, **(1992).**
19. Beck, J. S.; Calabro, D. C.; McCullen, S. B.; Pelrine, B. P.; Schmitt, K. D.; Vartulli, J. C. *U. S. Patent* 5, 145, 816, **(1992).**
20. Beck, J. S.; Kresge, C. T.; Leonowicz, M. E.; Roth, W. J.; Vartulli, J. C. *U.S. Patent* 5, 264, 203, **(1993).**
21. Beck, J. S.; Smith, K. D.; Vartulli, J. C. U.S. Patent 5,334,368, 1994. Beck, J. S.; Kresge, C. T.; McCullen, S. B.; Roth, W. J.; Vartulli, J. C. *U.S. Patent* 5,370,785, **(1994).**
22. Beck, J. S.; Vartulli, J. C.; Roth, W. J.; Leonowicz, M. E.; Kresge, C. T.; Schmitt, K. D.; Chu, C. T.-W.; Olson, D. H.; Sheppard, E. W.; Mc Cullen, S. B.; Higgins, J. B.; Schlenker, J. L. *J. Am. Chem. Soc.*, 114, 10834, **(1992).**
23. W.M. Meier, "Zeolite Structure" *Molecular Sieves*, Society for Chemical Industry, London, p. 10-25, **(1968).**

Co-ordinator

PRINCIPAL